Geophys. J. Int. (2008) **173,** 92–104 doi: 10.1111/j.1365-246X.2007.03711.x

Deep geoelectric structure over the Lower Brahmaputra valley and Shillong Plateau, NE India using magnetotellurics

S. G. Gokarn,[1] G. Gupta,[1] D. Walia,[2] S. S. Sanabam[2] and Nitu Hazarika[1]

[1]*Indian Institute of Geomagnetism, Kalamboli Highway, New Panvel-* 410218*, India*
[2]*Centre for Environmental Studies, North Eastern Hill University, Shillong-*793022*, India*

Accepted 2007 December 17. Received 2007 December 13; in original form 2006 March 10

SUMMARY

Magnetotelluric studies over the Shillong plateau and lower Brahmaputra sediments have delineated the Dauki fault as a NE–SW striking thrust zone with a dip angle of about 30°, along which the low resistivity layer of Bengal sediments and the underlying oceanic crust subduct to the northwest. At present, about 50 km length of these sequences has subducted beneath the Shillong plateau and is traced up to depth of about 40 km. Another thrust zone, sub parallel to the Dauki thrust is observed in the lower Brahmaputra valley, corresponding to the Brahmaputra fault. This is interpreted to be an intracratonic thrust within the Indian plate. These results suggest that a large fraction of the seismicity over the Shillong plateau is associated with the NE–SW striking Dauki thrust, contrary to the earlier belief that this fault zone is relatively aseismic. The present studies also suggest that the Shillong plateau and the adjoining sedimentary layers act as a supracrustal block, not directly participating in the subduction process. However in response to the compressive tectonic forces generated by the Himalayan and Indo-Burman subduction processes the Shillong plateau, together with the Brahmaputra sediments overlying the Indian crust drift eastwards relative to the Bengal sediments along the surface expression of the Dauki fault leading to a dextral strike slip movement. We thus propose that the NE Indian crust responds to the compressive forces differently at different depths, governed by the rheological considerations. At deeper levels the crustal readjustments take place through the subduction along the Dauki and Brahmaputra thrusts where as, at the shallow levels the relative deformability of the supracrustal blocks have a strong influence on the tectonics, leading to the strike slip mechanism along the surface expression of the Dauki fault.

Key words: Magnetotelluric; Seismicity and tectonics; Crustal structure; Asia.

INTRODUCTION

The NE Himalayan region is the seat of complex tectonic processes resulting from the dilatational tectonics active during the Triassic, when the Indian plate broke away from the Gondwanaland, followed by the Tertiary compressional tectonics due to the Indo-Eurasian and Indo-Burman collisions (Dasgupta & Biswas 2000). The century old great Shillong earthquake of 1897 that ruptured the Shillong Plateau (SP) is still a matter of intense debate at international level for several reasons. Although located in close vicinity of the confluence of two major collision zones, the causative factors resulting in this earthquake with an estimated magnitude of 8.7 on the Richter scale and focal depth of about 20 km, are traced to a hitherto ill-understood fault with a very small spatial extent of less than 200 km. Moreover, it occurred at a time when the seismic coverage was inadequate and the instrumentation was rather primitive and thus its source parameters are interpreted through the coseismic attributes, such as the geodetic levelling data, rupture zone, ground subsidence, etc. (Gahlaut & Chander 1992; Bilham & England 2001; Rajendran *et al.* 2004). The ensuing seismic monitoring (Khattri 1992; Kayal 1998; NEIC 2006) revealed a small and rather unsystematic cluster of intense seismic activity over the SP and the adjoining Lower Brahmaputra valley (LBV) distinct from the high seismicity associated with the Indo-Burman range. This is evident from the distribution of the earthquake foci reported on the NEIC (2006) WEB site, shown in Fig. 1 along with the known tectonic features in the NE Indian region. The irregular spatial and depth distribution of the seismic events is indicative of the complexity of the tectonic fabric in the SP and LBV region.

The Shillong Plateau and adjoining Mikir hills are the only exposures of the Archean-Proterozoic rocks in the entire NE Indian region, covered on all sides by the Tertiary sediments and the recent alluvium. It is believed that the rocks of the intermediate age may exist beneath the sedimentary cover of the Brahmaputra valley (Dasgupta & Biswas 2000). Thus most of the information on the deep interior of this region is hidden under the sedimentary cover and

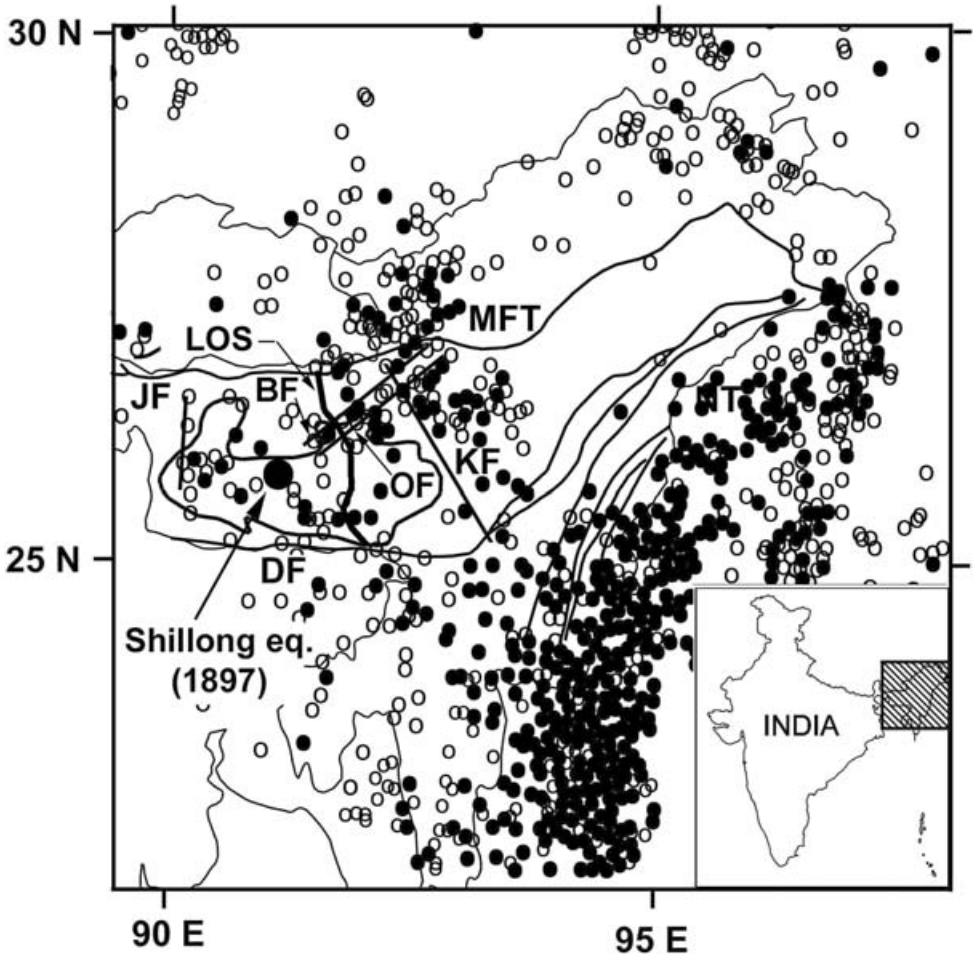

Figure 1. Tectonic map of NE Indian region, showing the epicentres of the shallow (depth of 33 km and less) and deep (more than 33 km depth) earthquakes. The deemed location of the 1897 Shillong earthquake is shown as a large solid circle. The location of the MT sites is shown as a thick solid line (marked, LOS). The major lineaments shown here are based on Kayal *et al.* (2006). JF: Jamuna fault, DF: Dauki fault, BF: Brahmaputra fault, OF: Oldham fault, MFT: Main frontal thrust, KF: Koppili fault.

is derived on the basis of the gravity studies and the interpretation of the geological features. Their nature and disposition is inferred from the source parameters and other seismological investigations, specific to a limited set of earthquakes in this region with closely spaced seismogenic faults. As a consequence, although the existence of the Brahmaputra, Oldham and Dauki faults finds a general acceptance, several conflicting arguments abound the scientific literature regarding the nature and the spatial and depth extent of these faults. The slickensides along the Dauki fault do suggest a right lateral strike slip motion (Evans 1964), but the vertical movements of the order of about 13 km of the crustal blocks relative to each other on either sides of this fault, indicated by a sharp drop of about 90 mGal in the Bouguer gravity (Fig. 2 redrawn from Verma & Mukhopadhyay 1977) favour a possible thrust hypothesis as advocated by several authors (e.g. Dasgupta 1977; Hiller & Elahi 1984). Controversies also exist about the Oldham fault, which was proposed by Oldham (1899) as the cause of the 1897 earthquake. Bilham & England (2001) suggest that this fault in the western SP has a southerly dip of 57°, where as, Rajendran *et al.* (2004) argue that no surface expression of the Oldham fault exists. Despite the strong need for the detailed understanding of the deeper crustal structure, there is an acute dearth of geophysical studies in this region, presumably due to the logistic difficulties in selecting suitable transects caused by the steep mountain slopes, the uncertain climatic conditions as well as the sporadic social disturbances which plague this region. The magnetotelluric (MT) studies over the SP and LBV region (Fig. 3) discussed here are an attempt at deciphering the manifestation of these tectonic features in the deep crust, which could prove useful in the systematic interpretation of the tectonic activity and crustal evolutionary processes.

GEOLOGY AND TECTONICS

The geological map of the study area and adjoining regions is shown in Fig. 3 along with the locations of the MT sites. The SP and the adjoining Mikir hills, known to be the detached portion of the Indian shield comprise the Archean to Proterozoic Gneisses and are covered by Quartzites, Grits and Slates, known as the Shillong series. Patchy remnants of a Tertiary cover and some unclassified crystallines are present in some parts of this plateau. The LBV to the north essentially consists of Alluvium, underlain by the Tertiary sediments. The Shillong rocks are expected to form the basement sequence in the LBV.

The Bouguer gravity map (Fig. 2, Verma & Mukhopadhyay 1977) shows gravity highs over the SP surrounded by predominantly negative values over the Bengal sediments to the south and southeast and

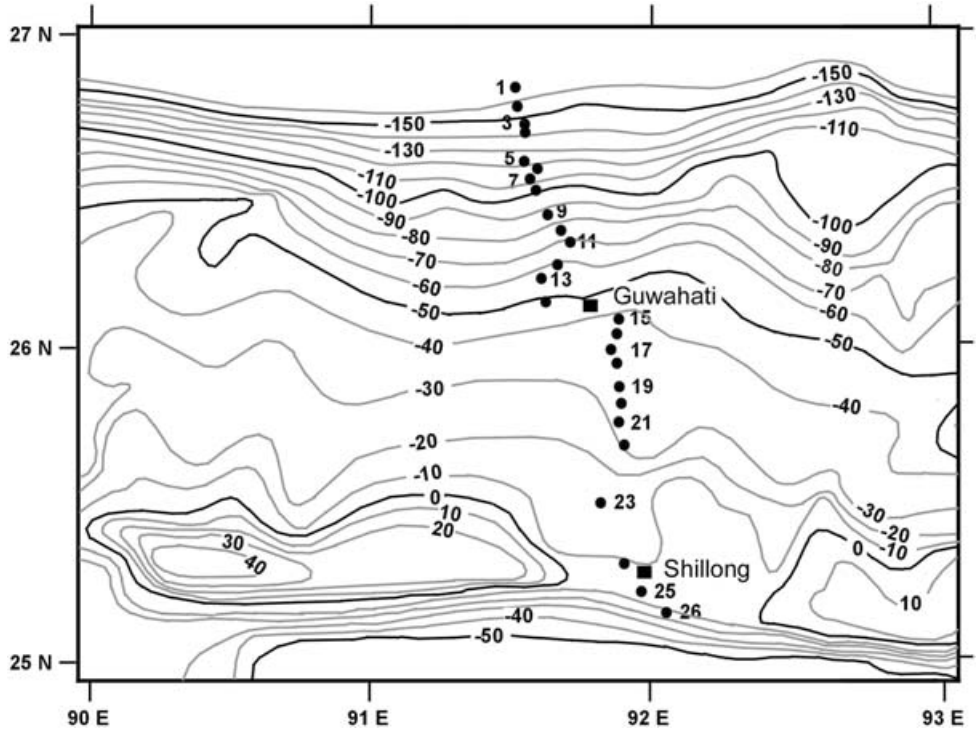

Figure 2. Bouguer gravity map of the SP and LBV showing the locations of the magnetotelluric survey sites. (After Verma & Mukhopadhyay 1977).

the Brahmaputra sediments to the north. Further north the gravity decreases consistent with the decreasing trend associated with the isostatic effects of the Himalayas (Verma & Mukhopadhyay 1977; Lyon Caen & Molnar 1983). Verma & Mukhopadhyay (1977) observe that the SP is itself isostatically uncompensated. The gravity highs over this plateau may not be entirely attributed to the absence of sedimentary overburden and hence these authors propose a high-density layer emplaced in the crust beneath the SP. The receiver function analysis (Mitra *et al.* 2005) delineate about 10 km thick high velocity layer beneath SP (*S*-wave velocity of about 4 km s^{-1}, as against 3.6 km s^{-1} in the surrounding region), which seems to support this conjecture. These studies suggest a crustal thickness of 38 km in the SP region and 42 km beneath the LBV.

Notwithstanding the strong influence of the sedimentary overburden on the Bouguer gravity, two prominent features attributable to the anomalies in the crust stand out here. The first is the NE–SW trending horst-like hump originating in the western part of SP running almost up to the 27°N latitude and the second, a NS feature in the eastern flank of SP, along the 90.6°E longitude.

Most of the seismic activity in the NE Indian region (Fig. 1) is associated with the Indo-Burman range, with the earthquake foci extending from shallow crustal levels to depths of about 200 km. A relatively small cluster of epicentres, distinct from the Himalayan and Indo-Burman seismicity is located over SP, LBV and some parts of the Himalayan thrusts. This cluster shows an unsystematic and rather confusing distribution of the epicentres. However a more systematic pattern emerges when the epicentres of the earthquakes with shallow (less than 33 km) and deep (33 km or more) focal depths are viewed along with the gravity contours, as shown in the Figs 4(a) and (b). Most of the shallow earthquakes especially near the MT sites are clustered around the NE-SW horst like gravity feature discussed earlier. Further NE, this trend is intercepted by the NW–SE line of epicentres, corresponding to the Koppili fault. Similar trend is apparent to some extent for the deeper foci, but is not very convincing. The rose diagrams of major tectonic features over SP region (Nandy 2001) are also suggestive of a NE–SW tectonic fabric in this region. Although seismic tomographic studies (Kayal 1998) show a rather unsystematic distribution of the seismic velocities at different depths over the SP and LBV, there is a reasonably clear indication of a NE–SW trend in the disposition of the *P*- and *S*-wave velocity differentials at depth of 16 km and greater.

Several studies exist on the seismicity associated with the Dauki fault. The fault plane solutions of six earthquakes in the close vicinity of the Dauki fault (Chen & Molnar 1990) indicate a thrust fault, with an oblique strike (NE–SW). These authors are of the view that these earthquakes with depths of about 50 km may not be related to the Dauki fault. Kayal *et al.* (2006) report a strike slip mechanism for two earthquakes at depth of 48 and 55 km near the Dauki fault.

It is evident from the foregoing discussion that the major fault systems in the SP and LBV are rather poorly understood and intensely debated regarding their nature and disposition. The root cause underlying these controversies is the fact that most of the fault systems are assessed on the basis of the source parameters of the specific seismic events in this complex tectonic setting with several closely spaced faults, thus rendering an inherent, event specific bias to the proposed models. The situation is further complicated because all the faults barring the Dauki fault are inaccessible for direct investigations. Magnetotelluric studies were conducted over a NS trending profile between Darranga (Bhutan border) to the north of the Himalayan frontal thrust and Dauki (Bangla Desh border) to the south. Due to the limitations set in by the international borders, only one site each was possible on south of Dauki fault and north of the Main frontal thrust (MFT).

FIELD SURVEY AND DATA ANALYSIS

Broadband MT data were collected at 26 sites over this 200-km-long linear profile using the Phoenix MTU-5A systems. Generally

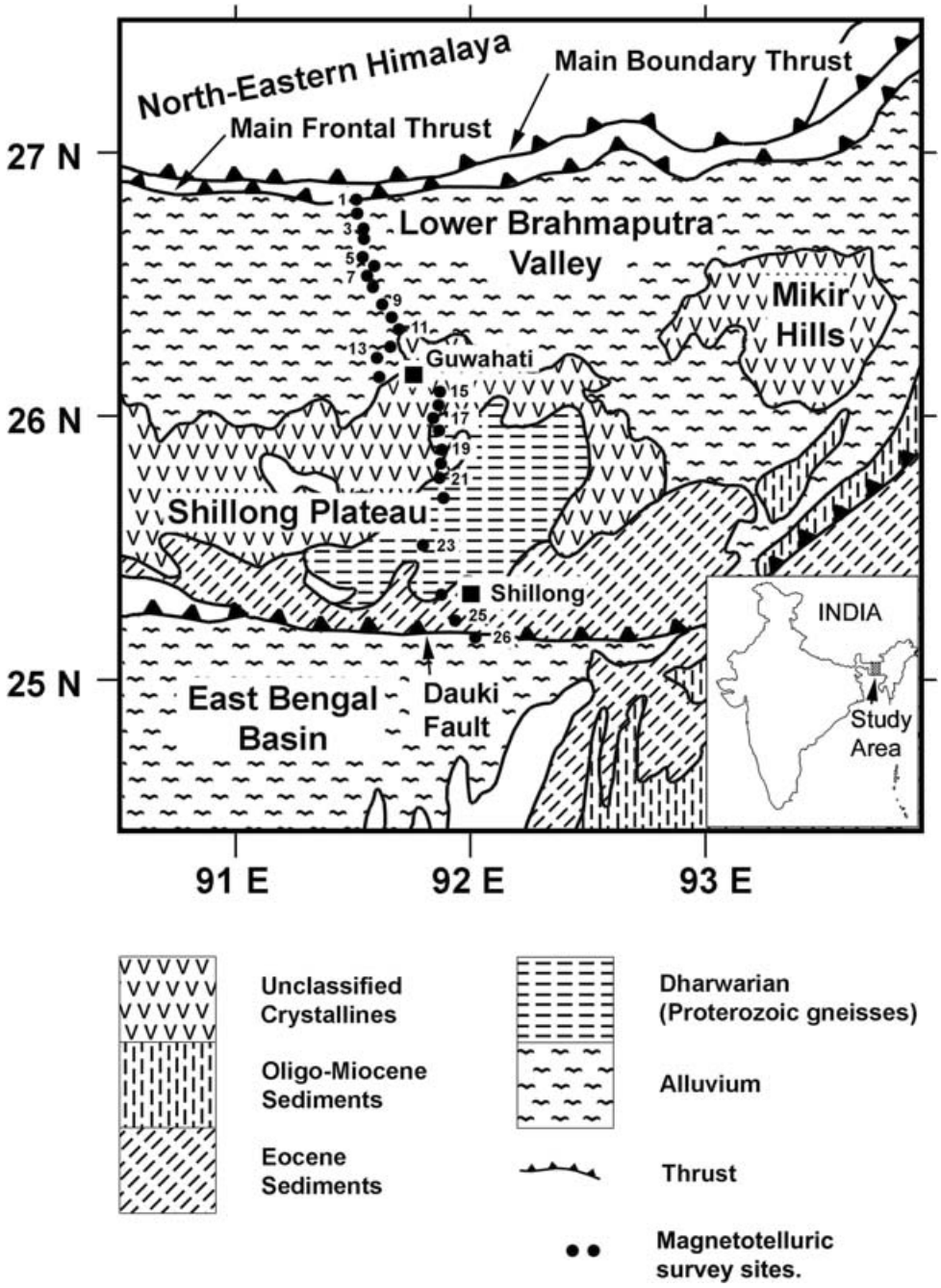

Figure 3. Geology of the SP and LBV showing the location of the magnetotelluric survey sites.

sites were chosen at intervals of about 5 km in the LBV region. However due to the limitations on the logistics set by the rugged topography with a dense forest cover, the site interval over SP was largely governed by the availability of suitable sites. Due to the high level of cultural noise around the township of Guwahati, no sites could be covered over a distance of about 20 km between the sites, 14 and 15.

The impedance tensors were obtained by using a combination of the fast Fourier transforms and cascade decimation procedure (Wight & Bostick 1980). In order to obtain the strike angles free from the near surface distortions, the impedance tensors were decomposed using the Groom Bailey procedure (Groom & Bailey 1989). Here the impedance tensors at all frequencies at each site were rotated at intervals of 5° to obtain the shear and twist for each rotation. This enables determination of the frequency invariant values of the shear and twist and also the range of the strike angles over which these parameters are reasonably stable. The shear and twist thus obtained at each site were fixed and the unconstrained strike angles were obtained at each frequency for all the sites. These values are shown at all the sites in Fig. 5 along with the observed strike angles averaged over frequency bands of one decade each. Most of the strike angles especially in the close vicinity of the major tectonic elements are aligned along the N45°E direction within a range of about 10°, suggesting a regional strike direction of NE–SW or perpendicular to it. The strike directions at some sites over the LBV region (Sites 7–11) show large variations. The geoelectric

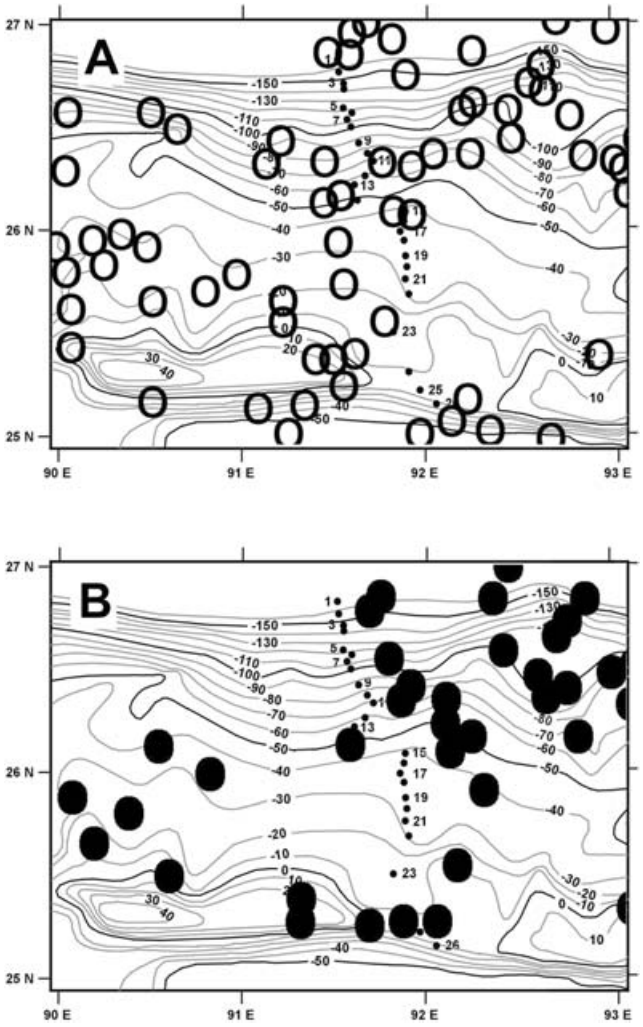

Figure 4. Seismic epicentres (from the NEIC WEB site, 2006) superimposed over the regional Bouguer gravity map of SP and LBV. (a) shallow, with depth of 33 km or less. (b) deep, with depth of more than 33 km.

strike has a weak dependence on the twist and shear and thus such large variations are not unusual. Furthermore the low resistivity top layer of sediments and alluvium tend to reduce the influence of the nearby vertical contrasts on the MT responses. The strike angles at the northern end of the profile (sites 1–3) could be constrained to N45°E with large shear values, in the range of 20–30°, indicating some three dimensionality, mostly arising out of the different strikes at the shallow and deep levels, in the close vicinity of the MFT. The region (sites 24 and 26) surrounding the Dauki fault to the south shows slightly larger twists of about 15°. The shear and twist however show reasonably small values at all the other sites over this profile, indicating largely a two dimensional structure with possible three dimensionality arising mostly due to the difference in the shallow and deep strikes. We thus treat the geoelectric structure as essentially two dimensional with a NE–SW strike (or perpendicular to it) and the effects of this assumption on the geoelectric structure will be considered at the interpretation stage. This assumption is not acceptable in the region to the north of MFT. However only one site is located to the north of the surface expressions of these features having a northerly dip and hence the effects of this assumption on the geoelectric structure will be assessed in the section on results and discussion.

Although the geology and the general alignment of the gravity contours show a predominantly EW strike, several studies discussed earlier which reflect on deeper tectonics such as the seismic epicentres (Fig. 4), velocity structure from the *P*- and *S*-wave tomography (Kayal 1998) as well as the exposed fault systems over the SP region (Nandy 2001), are indicative of a NE–SW strike at deeper levels. Thus the major trend suggesting the EW alignment of the gravity contours (Fig. 2) as well as the geological features seem to be controlled by the top sedimentary layer and may not correspond to the strike of the deeper tectonic features. The impedance tensors at all the sites were decomposed using the multisite, multifrequency Groom Bailey decomposition scheme proposed by McNeice & Jones (2001). Here the regional strike was constrained in the range of N35°E and N55°E, as indicated by the Groom Bailey decompositions at individual sites and a regional strike of N50°E was observed to be the best-fitting strike. The impedance tensors at all the frequencies and sites were rotated along this direction with the shear and twist constrained at the values obtained from the multisite, multifrequency tensor decomposition. The resultant rms misfit is shown in Fig. 5. The apparent resistivity and phase along this direction were assumed to be the TE-mode values and those perpendicular, the TM-mode values. The apparent resistivity and phase pseudo sections are shown in Figs 6 and 7, respectively. The forward modelled responses of the proposed geoelectric structure (Fig. 8) to be discussed in the next section are also shown here for comparison sake.

The effects of the static distortions caused by shallow surface inhomogenieties on the geoelectric structure were minimized by increasing the errors on the apparent resistivities by a factor of 100. This process decreases the weight of the apparent resistivity in the inversion and thus the resultant geoelectric section is largely controlled by the phase data, which are not affected by such shallow inhomogenieties. The true resistivity levels however cannot be defined by the phase data alone and thus the apparent resistivities with decreased weight have a sufficient control on the true resistivity levels; a presumption which needs to be ascertained after the inversion process.

The response functions were inverted using a two-dimensional inversion scheme (Rodi & Mackie 2001) using a half space with uniform resistivity as the initial model. The tau factor determines the smoothness of the iterated model in this inversion scheme, with the high values of this parameter leading to smoother models with relatively larger misfits where as the lower values result in smaller misfits at the cost of decreased smoothness. In such cases even the minor jitter in the observed responses can lead to unacceptable accumulation of high conductance in localized regions, which has adverse influence on the further convergence of the model. Thus the selection of these parameters needs to be optimized. The inversion was repeated with different resistivities of 50,100, 500 and 1000 ohm-m for the initial model and tau values of 5, 10 and 20. The model inverted using the uniform half space with a starting resistivity of 100 ohm-m and tau of 10 is found acceptable and is shown in Fig. 8 and the forward modelled pseudo-sections of the apparent resistivity and phase in the TE and TM mode for this model are shown in Figs 6 and 7, respectively, along with the observed Groom Bailey corrected responses for comparison sake. The rms misfit for this model was 1.9 after 180 iterations of the initial model.

The correspondence of the observed and modelled true resistivity levels was monitored by comparing them at the highest sounding frequency (320.0 Hz) as shown in Fig. 9. Here the observed resistivities in the TE and TM modes are denoted by solid and open circles, respectively. In the absence of any significant lateral

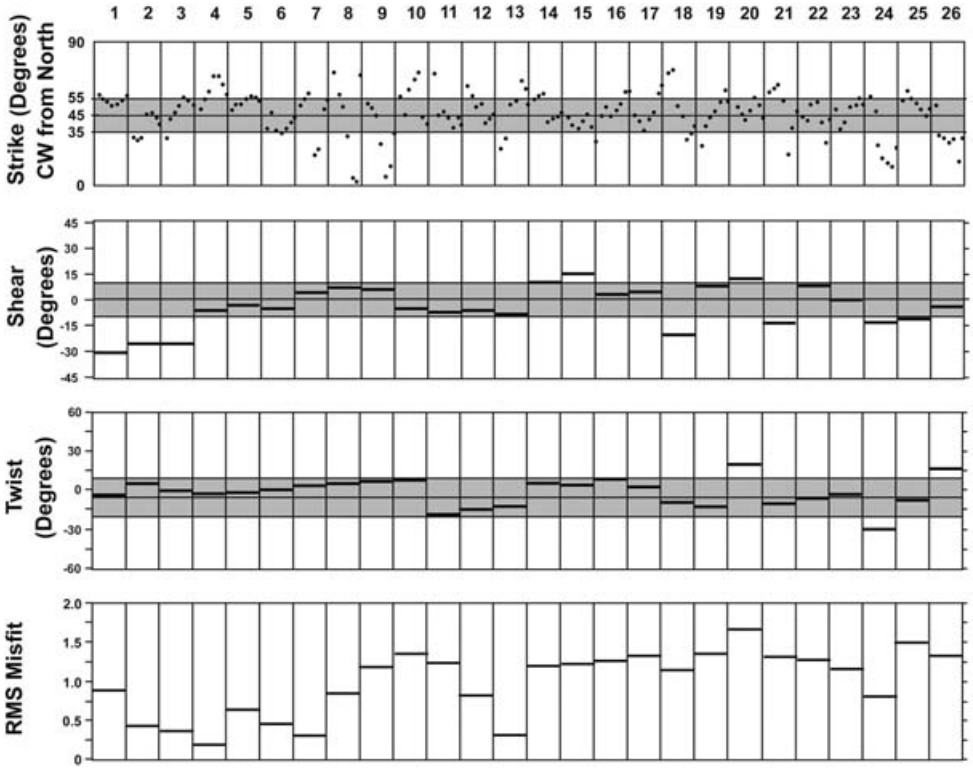

Figure 5. Spatial variation of strike in different frequency decades, shear, twist and the rms misfit from the multi site, multi frequency Groom Bailey decomposition along the MT profile in SP and LBV.

resistivity contrast, the forward modelled apparent resistivities in TE and TM modes at this frequency have similar values and hence both are denoted by only one curve here. The observed values are broadly clustered around the model curve, thus indicating that the downweighed apparent resistivities had sufficient control over the inversion process and the true resistivities in the geoelectric section.

RESULTS AND DISCUSSION

The geoelectric cross-section is shown in Fig. 8 along with the geological formations and locations of the surface expressions of the tectonic elements cut across by the MT profile reported in the recent literature (Kayal *et al.* 2006). For the convenience of discussion here, some high and low resistivity features in the geoelectric section are denoted by alphabets (A–H). In order to facilitate comparison with the MT responses, the signatures of these features are also marked in the phase pseudo-sections in Fig. 7 with the corresponding alphabets.

The high resistivity top layer 'D' between the sites 17 and 23 (Fig. 8) corresponds to the exposed part of the Shillong gneisses and the overlying layer of the unclassified crystallines in the northern part. This is indicated in the phase pseudo sections as low TE and TM phases (Fig. 7). This layer subducts northwards beneath a high resistivity layer 'B' along a high angle north dipping thrust. The intervening low resistivity layer 'C' may be due to the sediments which are subducting along with the Shillong gneisses. The TM as well as the TE phases have clear indication of this thrust, as is evident from the low phase, splitting into two branches to the north of site 11, one denoted as 'B' extending north and the other low phase branch below 'C' dips downwards. This thrust and its adjoining region to the north of the site 15 is covered by the Brahmaputra sediments 'A' deposited subsequent to commencement of thrusting. These sediments with a resistivity in the range of 10–20 ohm-m are rather thick, with a conductance of about 150 Siemens near the MFT at the northern end of the profile and gradually thin down towards the south up to site 15. As mentioned earlier, the regional strike direction chosen here does not correspond to the strike of the MFT where the Brahmaputra sediments are abut against the more resistive Siwalik sediments. Thus the conductance of 150 Siemens observed for the sediments in the vicinity of the MFT, may have been underestimated in the geoelectric section here. A cluster of low resistivity features occurring in patches ('H') are delineated at depth of about 20 km beneath the MFT. This low resistivity zone has clear signatures in the TM phase, although it is not seen in the TE phase. Studies in the other parts of the Himalayan orogen show similar low resistivities associated with the MFT (Reddy & Arora 1993; Gokarn *et al.* 2004a), suggesting that this is a regional feature, associated with this thrust and may be due to the accumulation of the saline fluids normally associated with the active thrusts (Jones 1992).

Kayal *et al.* (2006) propose the Brahmaputra fault beneath the LBV sediments bordering the SP to the north. On the basis of the fault plane solutions of two earthquakes these authors suggest that this fault may be a south dipping thrust. The location of the thrust zone denoted by 'C' and the high resistivity beneath coincides with the location of the Brahmaputra fault. However our observations above suggest that this fault is a NW dipping intracratonic thrust within the Indian plate and may have formed in the early stages of the Himalayan collision. The sedimentary layer subducting along this thrust zone indicates that about 30 km length of the crustal block may have been consumed here.

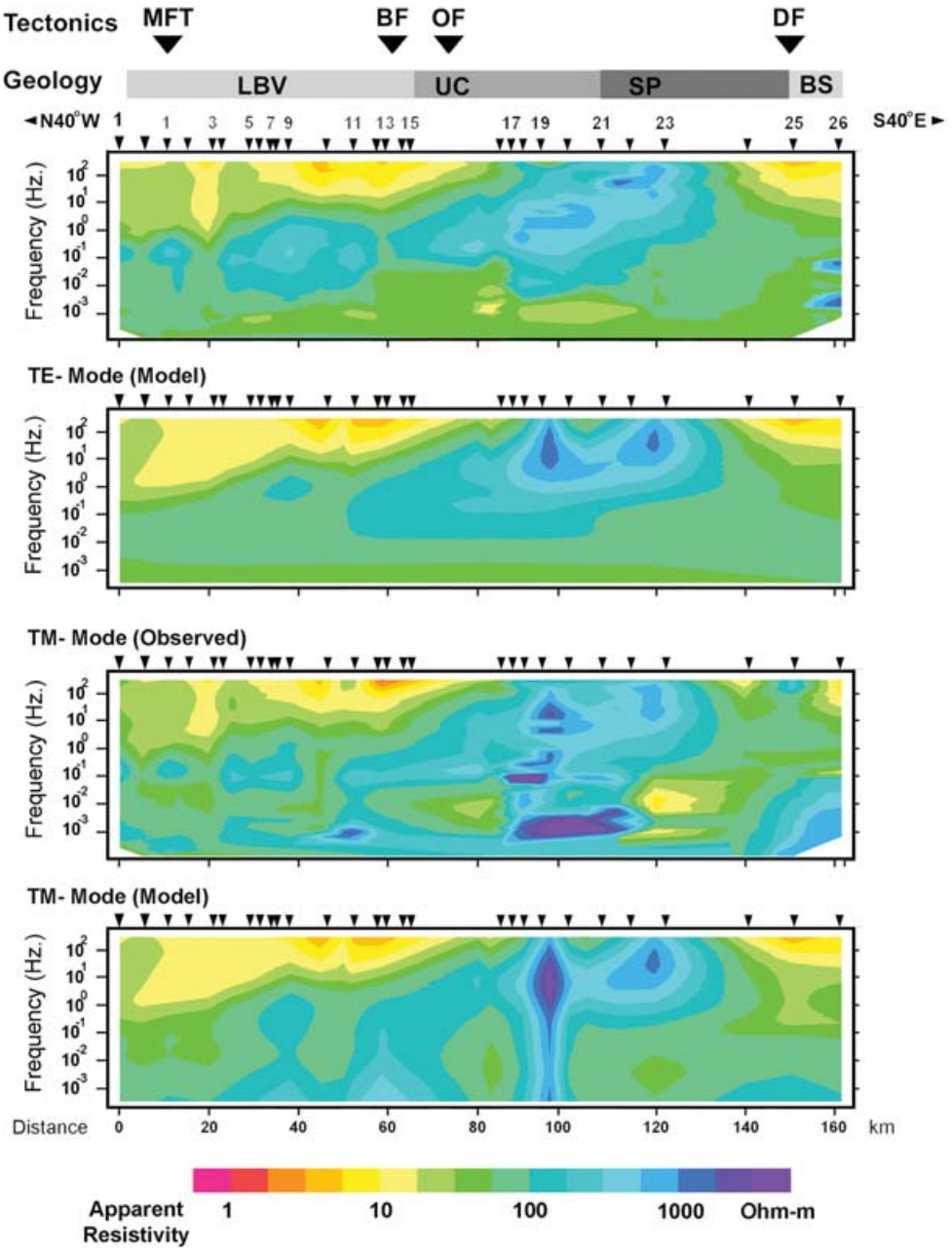

Figure 6. Observed and modelled apparent resistivity pseudo-sections over SP and LBV.

The Shillong Plateau extends to the south up to site 25 beyond which the low resistivity Bengal sediments are abut against it along the Dauki fault. The geoelectric section is suggestive of a NW dipping thrust with surface expressions near the site 25 along which the Bengal sediments and the underlying crustal block subduct beneath SP. The Bengal sediments delineated as the low resistivity layer 'E' are traced up to depth of about 15 km. This low resistivity layer is indicated in the phase pseudo-sections (Fig. 7) as the high phase 'E'. This is not clearly demarcated from the deeper high phase 'G', presumably because the intervening high resistivity layer may not offer sufficient conductance to be delineated in the response functions. Considering the fact that 'G' is located at depth of more than 25 km its signatures in the response functions are expected to be weak. Notwithstanding this fact an attempt is made here to ascertain the existence and fix the bounds of the resistivity of 'G' by testing the sensitivity of this feature. Here the 10, 20 and 50 ohm-m grid elements in 'G' were replaced with 100 ohm-m elements and the forward responses before and after the replacement were compared. The apparent resistivity and phase responses thus modelled at the sites, 15, 16, 21 and 22 are shown in Fig. 10 along with the observed responses from 60 hr long data sets. Here the solid lines correspond to the responses obtained using the model shown in Fig. 8 and the dashed lines are the responses of the model with 'G' replaced by the 100 ohm-m resistivity. The phases in both TE and TM modes show a maximum difference of about 7° between the two model responses and hence may not be suitable for constraining the resistivity range for 'G'. The apparent resistivity data however show significant frequency variations and will be used for addressing the sensitivity issue here. The apparent resistivities in the TE mode at low frequencies (<0.01Hz) at sites 15, 21 and 22 decrease

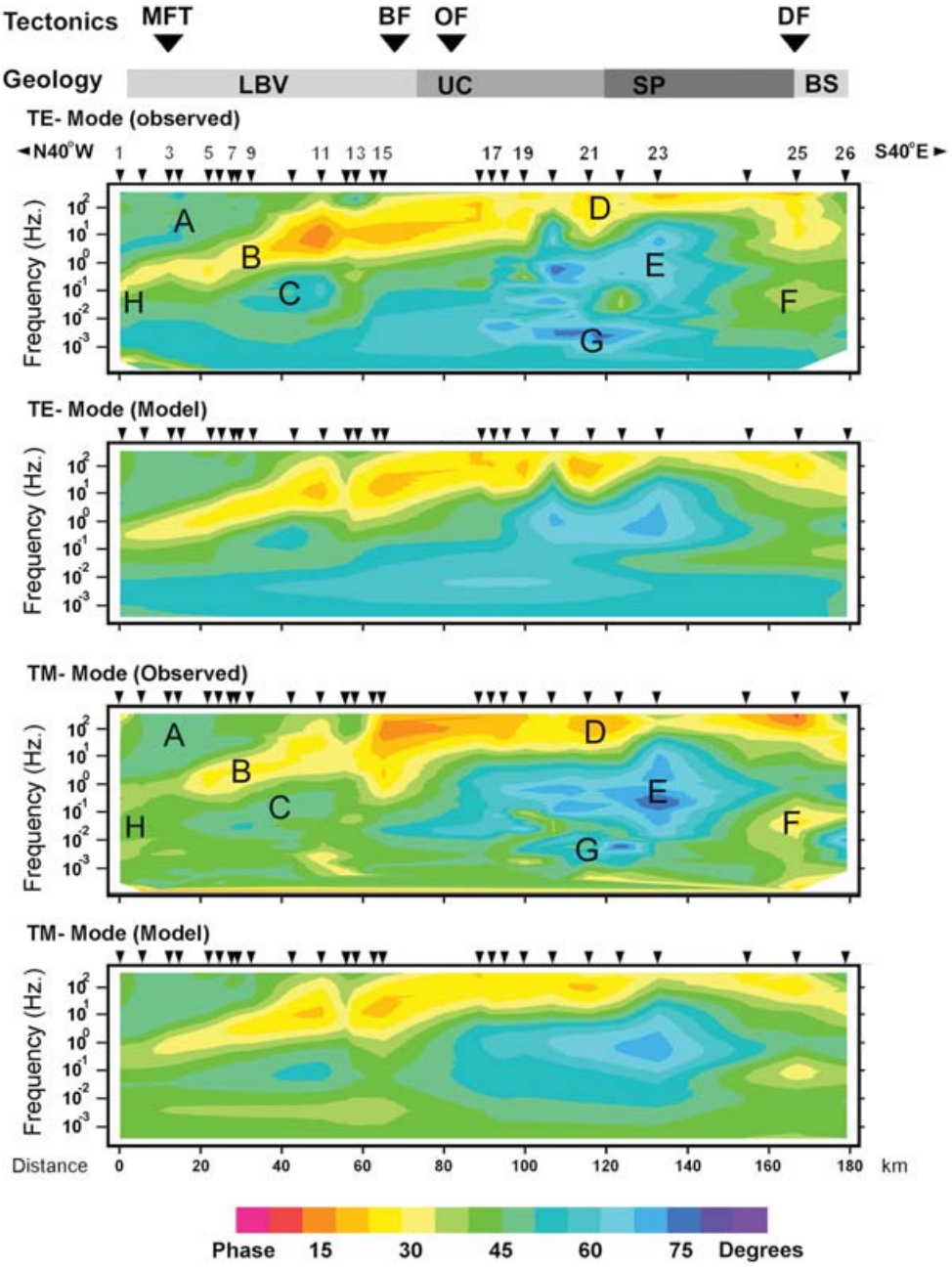

Figure 7. Observed and modelled phase pseudo-sections. The alphabets indicate the responses which may have major contribution to the resistivity features marked with the corresponding alphabets in the geoelectric model in Fig. 8.

more rapidly and are lower than the corresponding TM values by about an order of magnitude, although they have similar values at the high frequency end. This behaviour suggests that these sites are located on the resistive side of a lateral resistivity contrast at depths corresponding to these frequencies. Furthermore the apparent resistivities at the site 16 in both TE and TM mode decrease with the decreasing frequency in this range, suggesting that the site 16 is located on the top of 'G'. It may also be noted here that the apparent resistivities as well as phases at all sites obtained for the unaltered model (Fig. 8) show a better correspondence than those obtained after replacing 'G' with 100 ohm-m, which form the upper bound for the observed values. Thus the resistivity levels of 10–50 ohm-m for 'G' seem to be reasonably constrained by the observed apparent resistivities.

The Bengal sediments and the underlying crust from the south of SP seem to be subducting along the NW dipping thrust with the surface expressions at the site 25. This observation along with the other results such as, the presence of a 10 km thick high *S*-wave velocity layer (Mitra *et al.* 2005) and the high density beneath the SP surmised on the basis of the isostatic considerations (Verma & Mukhopadhyay 1977) along with the basaltic nature of the crust beneath the Bengal sediments (Baksi 1965; Sengupta 1966) suggests that the crust emplaced beneath SP along the thrust proposed here is oceanic in nature. The geoelectric section here indicates that about 50 km length of the oceanic crust may have been emplaced beneath SP at present.

The low resistivity 'G' is located at the dipping edge of the subducting oceanic crust and is delineated at depth of 20 km and beyond.

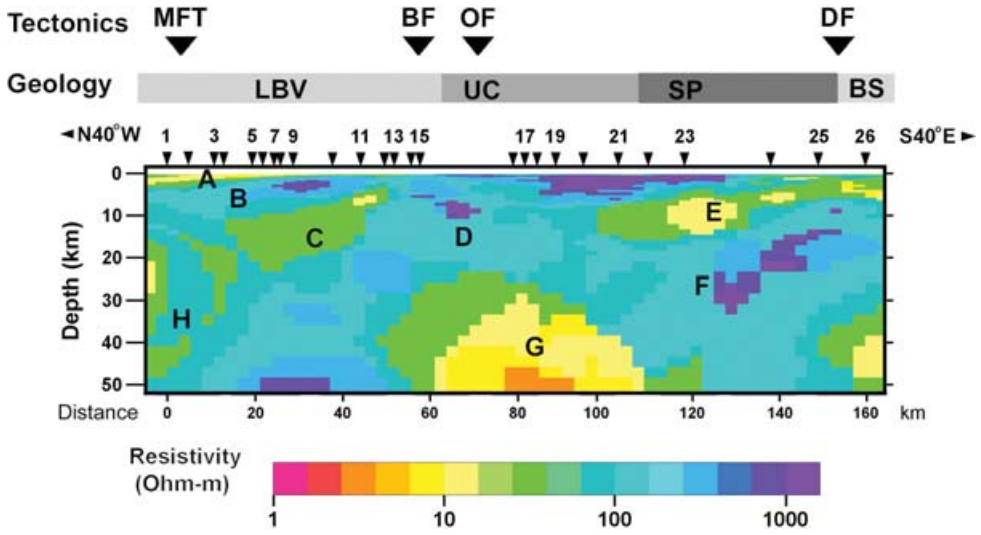

Figure 8. Geoelectric section over SP and LBV. The geology along the study profile is shown on the top part. Also marked are the surface expressions of the different tectonic elements (after Kayal *et al.* 2006). MFT: Main frontal thrust, BF: Brahmaputra fault, OF: Oldham fault, DF: Dauki fault and SP: Shillong plateau.

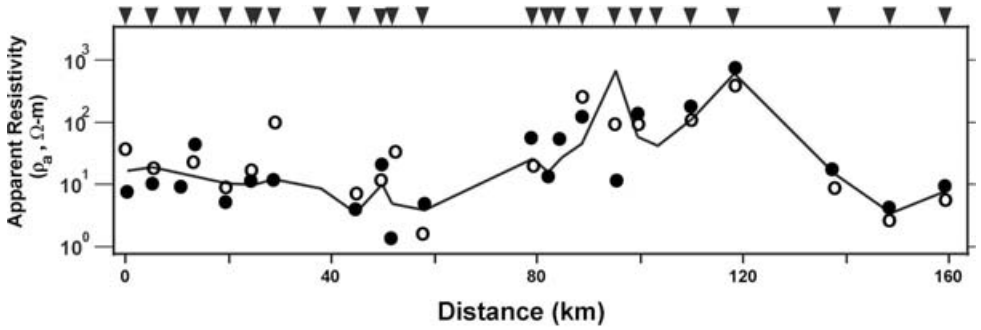

Figure 9. Observed and modelled apparent resistivity levels at 320 Hz. along the MT profile showing the effect of downweighing the apparent resistivity in the inversion process on the true resistivity levels. The solid and open circles denote the apparent resistivities in the TE and TM mode, respectively. The curve through the points denotes the forward modelled apparent resistivities in the TE and TM modes. The difference in the values in the two modes is not sufficient to be seen here.

Several mechanisms leading to a low resistivity in the deep crustal regime have been discussed by Jones (1992) such as the saline fluids, partial melts, grain boundary graphite films, geochemical sources such as the sulphides, pyrites, etc. Perhaps in an active subduction zone as is evident here, the saline fluids seem to be the best explanation for such low resistivity zones. Since the depth levels of this low resistivity are relatively shallow the possibility of partial melt is ruled out. Very few earthquake foci are located inside this low resistivity zone, as seen in Fig. 11, suggesting that the subducting crust may have generated liquid phase sufficient to prohibit the stress accumulation in this region.

Geoelectric cross-section viewed with other geophysical studies

To compare the geoelectric section and the interpretation above with the gravity studies, we created a density model based on the manually parametrized geoelectric section (Fig. 8). Here the known densities compiled by Verma and Mukhopadhyay (1977) are used for constraining the features 'A'-'E'. The densities of the deep features ('F', 'G', 'H' and 'I') are assumed values based on our interpretation. We have assumed a density value of 2.67 g cc^{-1} for the entire crust beneath LBV here because the receiver function analysis (Mitra *et al.* 2005) shows a uniform *S*-velocity of 3.6 km s^{-1}, up to depth of 40 km beneath the LBV without any intermediate layering. The gravity response of this model was compared with the observed response obtained from the Bouguer gravity contours (Fig. 2). The final density model obtained by manually modifying the model parameters is shown in Fig. 12 along with the modelled and observed gravity values on the top part of the figure for comparison sake. The gravity was computed using the program GRAV2DC, (available on the web site, http://www.rockware.com). Most of the misfit could be reduced by modifying the thickness of the low resistivity sedimentary layers ('A', 'C' and 'E'). This modification seems acceptable because the bottom of the low resistivity layers is not well-constrained parameter in the geoelectric models and thus there is always an uncertainty associated with such interphases. Perhaps a more significant modification is the assignment of the low density value of 2.52 g cc^{-1} to 'G' and 'H', which supports the existence of the fluid filled fractures that may have caused the low resistivities. Thus the model proposed here seems to adequately explain the gravity field over the SP and LBV regions.

In order to assess the seismicity over the various resistivity features in a comprehensive manner, the seismological data from different available sources are compared with the geoelectric section

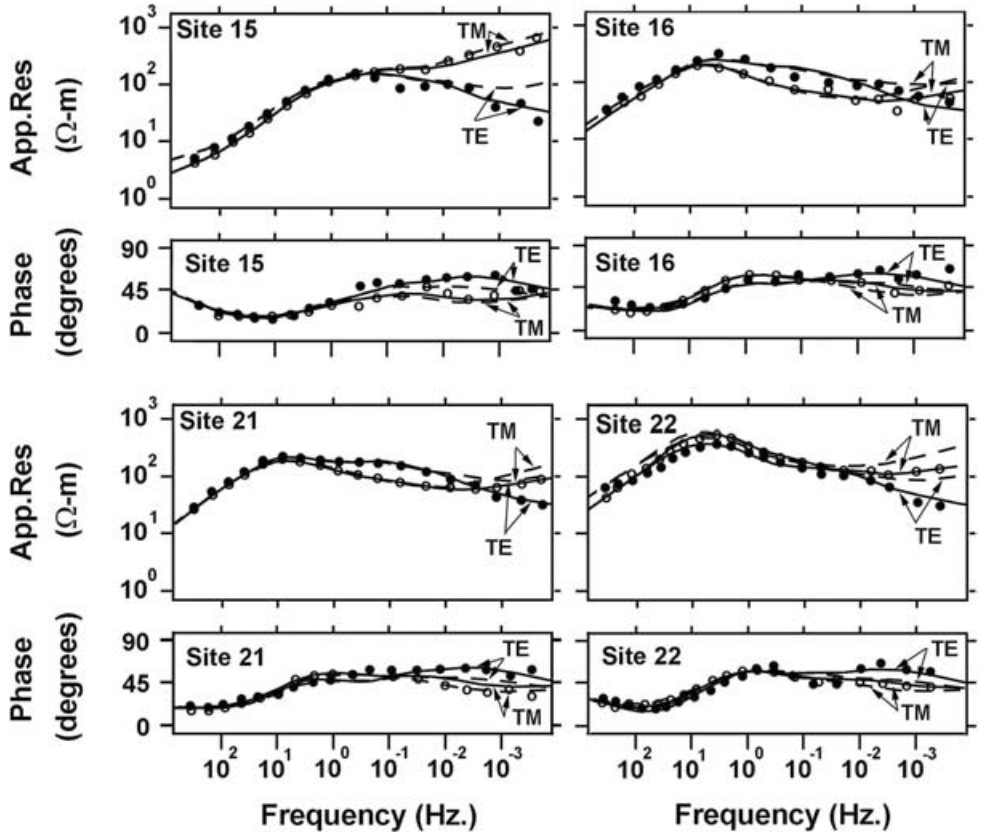

Figure 10. Forward modelled apparent resistivity and phases at sites, 15, 16, 21 and 22 before (continuous curves) and after replacing (dashed curves) the low resistivity layer 'G' (in Fig. 8) with resistivity of 100 ohm-m. Also shown here are the observed data points of the corresponding responses. Solid circles are the TE mode values and open circles, the TM mode values.

here. The foci of earthquakes recorded by the regional seismic array from the NEIC (2006) WEB site in the longitude band between 91.5°E and 92.5°E which encloses the MT survey profile, are plotted over the geoelectric cross-section in Fig. 11(a). In all 53 events are reported on the NEIC (2006) WEB site as of 2006 June. About 28 of these show a depth of 33 km, which seems to be the default (uniterated) depth value and hence these are not shown here. The seismic activity along the Brahmaputra thrust proposed in the geoelectric section with a northerly dip is clearly indicated in the five seismic events aligned along this line beneath the sites 1 and 9 in the depth range of 35–50 km. However only three events are located in the SP region and only one seems to be located on the subducting Dauki thrust.

The epicentral distribution from the local microseismic array reported by Khattri (1992) provides a dense distribution of the earthquake foci in the longitude band of 90°E and 92°E. These are superimposed on the geoelectric section in Fig. 11(b). Most of the earthquake foci are distributed in and around the Dauki thrust proposed here. This observation suggests that perhaps this feature which was earlier known to be aseismic (Rajendran *et al.* 2004) may account for most of the seismicity in the SP region. The earthquake foci seem to be spread over almost a 50 km wide band in the vicinity of this thrust, suggesting that the Dauki fault is an en echelon thrust system or that some other faults which have no significant expression in the geoelectric section may exist in its close vicinity.

Recently, Kayal *et al.* (2006) have reported the focal plane mechanisms over several earthquakes in the NE Indian region. The locations and dip of the focal planes of the earthquakes in the SP region are shown, superimposed over the geoelectric section in Fig. 11(c). The tectonic features inferred from the present studies are also shown in this figure for comparison sake. Here the location of the earthquake foci located between 91°E and 92°E, which are in the close vicinity of the Dauki thrust are shown along with the corresponding focal planes reported by Kayal *et al*. (2006). The fault planes of two of the three earthquakes (denoted as 6 and 7) show a NW dip, although the dip angles are different from the dip of the Dauki thrust proposed here. The third earthquake (denoted as 8) does not show any correspondence to the Dauki thrust.

CONCLUSIONS

The tectonics in the SP, LBV and adjoining regions of the NE India is essentially the response of lithospheric blocks to the compressive tectonic forces generated by the northward subduction of the Indian plate along the Himalayan thrusts and its eastward thrusting along the Arakan Yoma thrust. The EW component of these compressive forces is generated by the anticlockwise rotation of the Indian plate subsequent to its first contact with the Eurasian plate at the Pamir node (Raval 2000). As a result the entire NE Indian region is being pushed into the wedge formed by the two major mutually orthogonal thrust zones. The consumption of the Indian lithosphere along these two thrusts does not seem to be adequate for effectively containing the stresses generated by the compressive tectonics and thus the residual stresses accumulate in the NE Indian crust. In view of the complexity of the tectonics in this region, the discussion here

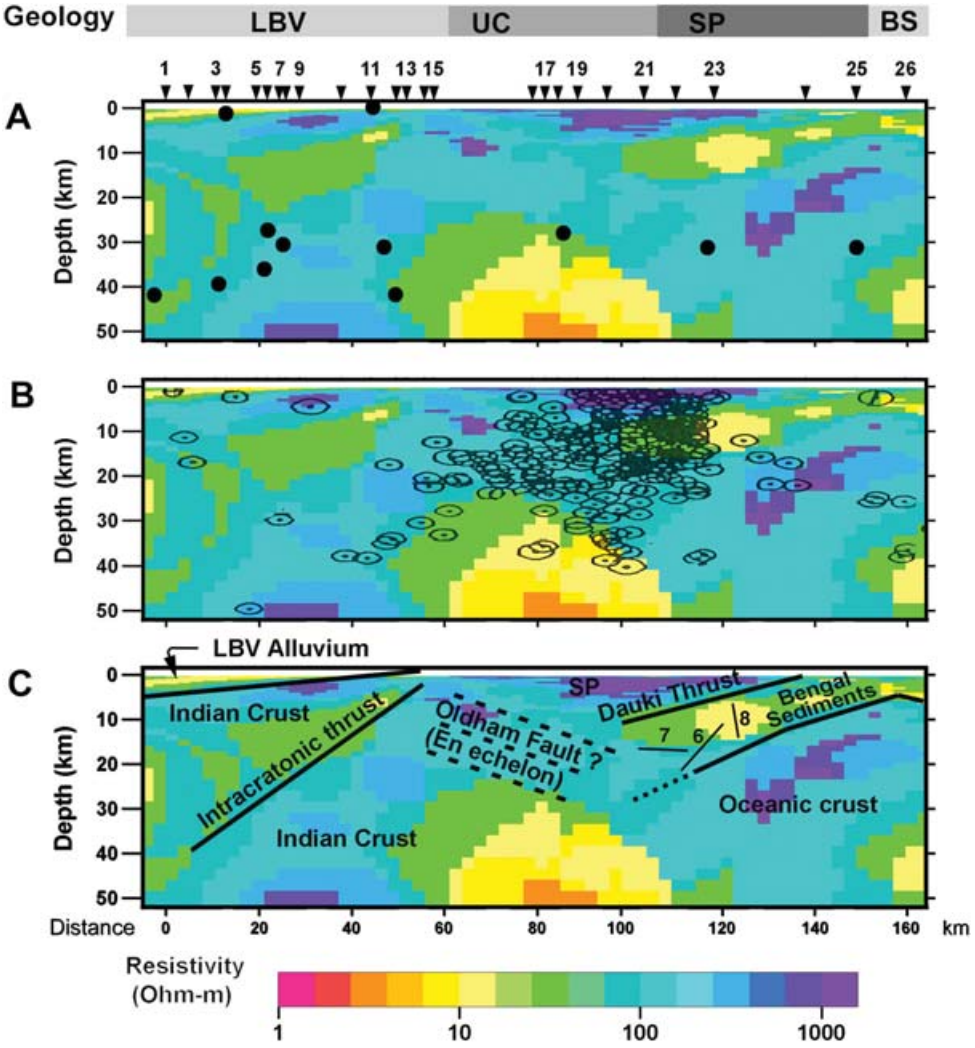

Figure 11. Geoelectric cross-section over SP and LBV, superimposed with the depths of foci of the earthquakes from the different available sources. (a) foci in the longitude band between 91.5°E and 92.5°E, (NEIC 2006), (b) foci in the longitude band between 90°E and 92°E, reported by Khattri (1992) and (c) dip direction obtained from the fault plane solutions for the earthquakes in the longitude band between 91°E and 93°E (Kayal *et al.* 2006). The tectonic elements and the rock types, deciphered from the present study are also shown in this part of the figure for comparison sake.

is restricted to the SP and LBV, delimited by the Koppili fault to the east and the Jamuna fault to the west (Fig. 1). The NE Indian crust seems to respond differently to the accumulated stresses at different depth levels. The Shillong block and some part of the adjoining sedimentary layers together forms the shallow crustal block comprising rocks of widely differing ages and rheologies. The lithosphere beneath this shallow crustal block subducts along the Dauki thrust and the intracratonic Brahmaputra thrust. The geoelectric structure here suggests that so far, at least about 50 and 30 km length (along NW–SE direction) has been consumed along the Dauki and Brahmaputra thrusts, respectively. The shallow crustal block does not participate in the subduction process and is pushed laterally in response to the compressive forces. The observed EW dextral strike slip along the surface expression of Dauki fault at shallow levels suggests that the hardened rocks of the Archean SP, which were a part of the Indian plate till recent times, have moved eastwards in relation to the easily deformable sequences of Bengal sediments. Some stresses to the south and east of the SP are also absorbed along the Arakan Yoma and other fold belts as well as in the crust beneath (Gokarn *et al.* 2004b). The Brahmaputra sediments to the north of SP, overriding the Indian crust experience relatively low level of compressive stresses, which are released through the microseismic activity.

The distribution of the supracrustals over SP (Fig. 3.), with predominantly the Eocene sediments to the south up to the Dauki fault and their absence in the northern part suggests that perhaps this plateau had a southward slope as against the nearly horizontal disposition observed at present. Apart from the tectonic uplift, the thickening of the juvenile oceanic crust subducting northward beneath the Dauki thrust may also have contributed to the differential uplift of the SP. In view of the intense weathering and the transportation of the Shillong group rocks in to the Surma valley to the south (Nandy 2001), it may not be feasible to estimate the relative uplift. Nevertheless, this is indicative of possible flexural strains in the hard rocks of the SP in addition to the residual strains originating from the tectonic processes discussed earlier.

The Oldham fault at the northern margin of SP is not delineated in the geoelectric section presented here, although two low resistivity features with a rather weak resistivity contrast of a factor of 5 (100 ohm-m against the surrounding resistivity of 500 ohm-m), are delineated, extending over four sites (16–19) which are not clearly

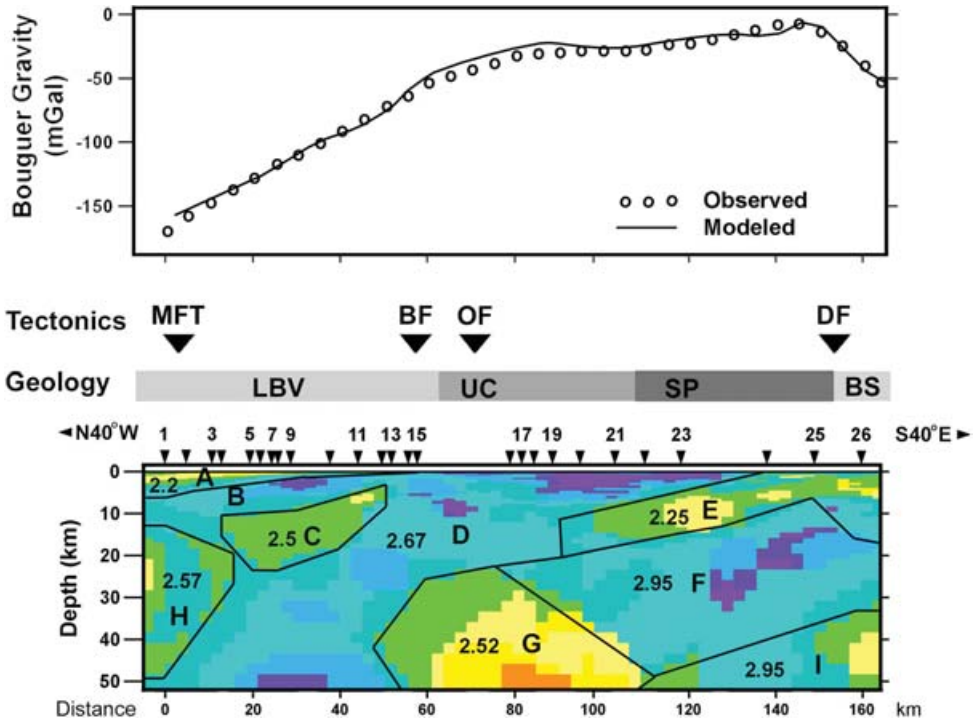

Figure 12. Density model for SP and LBV proposed on the basis of the geoelectric model. The numbers on the tectonic units indicate the density values in g cc^{-1}. The forward gravity response is shown on the top part of the figure along with the regional Bouguer gravity. The colour scale is same as that for Fig. 8.

indicated in the phase pseudo-sections in Fig. 7. The coverage between the sites 15 and 16 is insufficient to address to this problem. A denser site spacing was not feasible in this region because of the strong cultural noise caused by the Guwahati township and hence this low resistivity could not be effectively delineated. A comparative assessment of the geoelectric cross-section together with the distribution of the earthquake foci observed from the local seismic network (Fig. 11b) shows a rather large scatter of more than 50 km around the Dauki thrust proposed here. This may not be entirely attributable to the Dauki thrust. A closer observation of the foci also suggests two sub-parallel trends with a southerly dip at depth of about 10 and 20 km beneath the site 16, which may not be associated with the north dipping Dauki thrust and thus may be indicative of the Oldham fault. Perhaps this fault may be a reverse fault or a back-thrust caused by the northerly push of the Shillong plateau by the subducting oceanic plate. From the absence of any sediments subducting along this fault or any significant movements on either sides, this fault seems to be a recent addition to the tectonics of this region.

The deemed location of 1897 earthquake (Fig. 1) is at a distance of about 70 km to the west of the present study profile. More important it is located on the westward projection (along the strike direction of NE–SW) of the Dauki thrust at depth of about 20 km, the estimated focal depth of the 1897 earthquake, as well as the epicentral line of the earthquakes in the SP and LBV region (Fig. 1). Kayal & De (1991) propose that the westward extension of the Dauki thrust may be responsible for the 1897 earthquake, which seems to be corroborated by the present studies. The MT studies presented here are a part of a major project undertaken by us to cover several other parts of the NE Indian crustal block, which also includes a profile in the epicentral region of the 1897 earthquake and another to the east of the Koppili fault. Perhaps these future studies will enable a more definitive suggestion in this regard.

ACKNOWLEDGMENTS

The authors are grateful to the Seismicity and the Deep Continental Studies programmes of the Earth System Science Division, Department of Science and Technology (DST), Govt. of India for funding this study. Special thanks to Drs G.D. Gupta and K.R. Gupta, Advisors, DST for their interest and encouragement. The authors also express their gratitude to Prof A. Bhattacharyya, Director, Indian Institute of Geomagnetism for her keen interest in these studies. Thanks to Ms. Shipra Dutta for the help in field surveys. Grateful thanks to Prof Alan Jones for providing the multisite, multifrequency strike determination program. The authors are indebted to Prof Martyn Unsworth and the other anonymous reviewers for the critical comments and excellent suggestions.

REFERENCES

Baksi, S.K., 1965. Stratigraphy of the Barail series in the southern part of the Shillong Plateau, Assam, India, *Am. Assoc. Pet. Geol. Bull.,* **49,** 2282–2294.

Bilham, R. & England, P., 2001. Plateau pop up in the great Assam earthquake, *Nature,* **410,** 806–809.

Chen, W.-P. & Molnar, P., 1990. Source parameters of the earthquakes and Interplate deformation beneath the Shillong Plateau and Northern Indo-Burman ranges, *J. geophys. Res.,* **95**(B8), 12 527–12 552.

Dasgupta, A.B., 1977. Geology of Assam-Arakan region, *Oil Comment., India,* **15,** 4–34.

Dasgupta, A.B. & Biswas, A.K., 2000. *Geology of Assam*, pp. 170, Geol. Soc. of India, Bangalore, India.

Evans, P., 1964. The tectonic framework of Assam, *J. Geol. Soc. India,* **5,** 80–96.

Gahalaut, V.K. & Chander, R., 1992. A rupture model for the great earthquake of 1897, northeast India, *Tectonophysics,* **204,** 163–174.

Gokarn, S.G., Gupta, G., Walia, D. & Dutta, S., 2004a. Magnetotelluric studies in the Sikkim Himalaya, Poster presented at the *17th International*

workshop on the electromagnetic induction in the Earth, Hyderabad, India, 18–23 October, 2004.

Gokarn, S.G., Gupta, G., Walia, D. & Selvaraj, C., 2004b. Magnetotelluric studies in the Arakan Yoma fold belts in Mizoram, India, Poster presented at the *17th International workshop on the electromagnetic induction in the Earth*, Hyderabad, India, 18–23 October, 2004.

Groom, R.W. & Bailey, R.C., 1989. Decomposition of the magnetotelluric impedance tensor in the presence of local three dimensional galvanic distortions. *J. geophys. Res.,* **94,** 1913–1925.

Hiller, K. & Elahi, M., 1984. Structural development and hydro-carbon entrapment in the Surma Basin, Bangladesh (northwest Indo–Burman Fold belt). in *Proc. 4th Offshore Southeast Asia Conference*, Singapore, pp. 6.50–6.63.

Jones, A.G., 1992. Electrical properties of the lower continental crust, in *Continental Lower Crust*, pp. 81–144, eds Fountainhead, D.M., Arculus, R. & Kay, R.W., Publ: Elsevier, Netherlands.

Kayal, J.R., 1998. Seismicity of northeast India and surroundings—development over the past 100 years, *J. Geophys.,* **XIX**(1), 9–44.

Kayal, J.R. & De, R., 1991. Microseismicity and tectonics in the northeast India, *Bull. seism. Soc. Am.,* **81,** 131–138.

Kayal, J.R., Arefiev, S.S., Barua, S., Hazarika, D., Gogoi, N., Kumar, A., Chowdhury, S.N. & Kalita, S., 2006. Shillong plateau earthquakes in northeast Indian region: complex tectonic model, *Curr. Sci.,* **91**(1), 109–114.

Khattri, K.N., 1992. Seismological investigations in north eastern region of India, *Mem. Geol. Soc. India,* **23,** 275–302.

Lyon Caen, H. & Molnar, P., 1983. Constraints on the structure of the Himalaya from an analysis of the gravity anomalies and a flexural model of the lithosphere, *J. geophys. Res.,* **88,** 8171–8191.

McNeice, G.W. & Jones, A.G., 2001. Multi-site, multi-frequency tensor decomposition of magnetotelluric data, *Geophysics,* **66,** 158–173.

Mitra, S., Prestley, K., Bhattacharyya, A.K. & Gaur, V.K., 2005. Crustal structure and earthquake focal depths beneath northeastern India and south Tibet, *Geophys. J. Int.*, doi: 10.1111 j.1365-246X2004.02470.x

Nandy, D.R., 2001. *Geodynamics of Northeastern India and the Adjoining Region*, pp. 209, ACB, Publ., Kolkata.

NEIC, 2006. WEB page, http://www.neic.usgs.gov

Oldham, R.D., 1899. Report of the great earthquake of 12th June, 1897, *Mem. Geol. Soc. India*, pp. 379.

Rajendran, C.P., Rajendran, K., Durrah, B.P., Barua, S. & Earnest, A., 2004. Interpreting style of the faulting and palaeoseismicity associated with 1897 Shillong, NE India earthquake; Implications on regional tectonism, *Tectonics,* **23,** TC 4009, doi: 10.10 29/2003TC001605.

Raval, U., 2000. Laterally heterogeneous seismic vulnerability of the Himalayan arc: a consequence of cratonic and mobile nature of underthrusting Indian crust, *Curr. Sci.,* **78,** 546–549.

Reddy, C.D. & Arora, B.R., 1993. Quantitative interpretation of geomagnetic induction response across the thrust zones of Himalaya along the Ganga Yamuna valley, *J. Geomag. Geoelectr.,* **45,** 775–785.

Rodi, W. & Mackie, R.L., 2001. Nonlinear conjugate gradients algorithm for 2D magnetotelluric inversions, *Geophysics,* **66,** 174–187.

Sengupta, S., 1966. Geological and Geophysical studies in the western part of the Bengal basin, India. *Am. Assoc. Petr. Geol. Bull.,* **50,** 1001–1017.

Verma, R.K. & Mukhopadhyay, M., 1977. An analysis of gravity field in the north eastern India, *Tectonophysics,* **42,** 283–317.

Wight, D.E. & Bostick, F.X., 1980. Cascade decimation–a technique for real time estimation of power spectra, *Proc. IEEE International conf. Accoustic, Speech Signal Processing*, pp. 626–629, Denver, Colorado, April, 9–11, 1980.